Lead Titanate films on Dysprosium Scandate with a Strontium Ruthenate Buffer Layer grown by Pulsed Laser Deposition

By: Brian Smith

November 2009

Supervised by: Beatriz Noheda

Abstract

Ferroelectric materials play an important role in modern technological applications. Device miniaturization and integration with current semiconductor processing technology require the use of ferroelectric thin films for many future applications. The domain structure of a ferroelectric thin film will have a large influence on the properties of the film. This paper investigates the domain structure of $PbTiO_3$ films of varying thicknesses, from 24 to 44 nm, grown on a $DyScO_3$ substrate with a $SrRuO_3$ electrode layer. $DyScO_3$ is chosen as the substrate due to small misfit strain with $PbTiO_3$ at high temperatures and it has a room temperature misfit strain near the critical boundary for 90° domain formation. The films are grown using pulsed laser deposition with reflection high energy electron diffraction to monitor the film growth. A number of techniques such as reciprocal space mapping, atomic force microscopy, and piezoresponse force microscopy are used to determine the domain structure and the domain periodicity of the films. The results show that for the film thicknesses investigated there is a linear dependence on the domain periodicity as a function of film thickness. This dependence is not in agreement with theoretical predicted square root dependence. The results are then compared with the theoretical results of Pertsev and Zembilgotov who predict a linear dependence over a certain thickness regime.

Table of Contents

1. Introduction

The first ferroelectric material was discovered in the 1920s. It wasn't until the discovery of ferroelectricity in $BaTiO_3$ in the 1940s that interest in ferroelectricity developed beyond mere scientific curiosity [1]. The chemical and physical robustness of $BaTiO_3$'s perovskite structure allowed experimental studies to be preformed while its relatively simple crystal structure, compared with previous ferroelectrics, enabled theoretical studies. Today, ferroelectric materials play an essential role in modern technology. Applications of thin film ferroelectrics include nonvolatile memories, microelectronics, electro-optics, and electromechanical systems [2]. Development of ferroelectric thin films began in the late 1960's for use as nonvolatile memories. Despite the promise of these thin films, research was stifled by difficulties processing and integrating ferroelectric films. As a result little progress was made until the 1980's [3]. At this time improvements in processing of thin film ferroelectric oxides allowed high quality films to be grown for research and applications.

Incorporating ferroelectrics into current electronic devices requires the ferroelectrics to be processed using semiconductor processing techniques. These techniques require the ferroelectrics be thin films so it is essential to understand how the ferroelectric behavior changes when the material is a thin film. Studying thin film ferroelectrics is not just important for device applications. Ferroelectric thin films also provided scientists with unique opportunities to examine the fundamental nature of ferroelectricity. Processing of ferroelectric thin films has advanced to the point where it is possible to create films with thicknesses of less than 100nm. At these thicknesses it becomes possible to create atomistic models for the entire film allowing both theoretical and experimental studies. Having a common ground between theory and experiment allows a feedback between the two groups which has resulted in rapid progress in this field.

Another unique feature of thin films is the ability to grow them epitaxially on substrates. When there is a mismatch between the lattice parameters of the substrate and the ferroelectric, the film becomes strained. The amount of strain in the film will depend on the exact mismatch between lattice parameters of the film and substrate. Many properties of a ferroelectric depend on the amount of strain in the material. "Strain engineering" is often used to tune the properties of a ferroelectric thin film by growing films on substrates with different lattice parameters. The strains that are incorporated by the ferroelectric thin film are much greater than what is possible in a bulk ferroelectric of the same material. Thin films, therefore, allow access to previously unattainable strain dependent properties

The properties of a ferroelectric film depend greatly on the structure of the domains in the film. The domain structure will have a great impact on the dielectric, piezoelectric and optical properties of the film [3]. In order to obtain the optimal properties for specific applications it is necessary to control the domain structure in the film. Different applications of ferroelectric thin films take advantage of different properties of the film. As a result the desired domain structures will vary depending on the application. For example, ferroelectric films used in nonvolatile memories need to have high remnant polarization which is achieved by domains with out of plane polarization. Conversely, domains with polarization in the plane of the film are desired for use as capacitor devices where this domain structure increases the dielectric constant of the film [2].

Controlling the domain structure of epitaxial ferroelectric thin films is vital if such films are to continue to play an important role in practical applications. This paper will explore the domain structures of $PbTiO_3$ ferroelectric thin films grown on $DyScO_3$ substrates with a $SrRuO_3$ electrode layer. High quality films of varying thickness are grown using the Pulsed Laser Deposition technique. X-ray diffraction, atomic force microscopy, and

peizoresponce force microscopy are used to characterize the films. The domain periodicity as a function is determined and compared with theoretical models.

2. Background

2.1. Thin Films:

When a single crystalline film is grown on a single crystal substrate, there is often a strong relation between the lattices of the two crystals. The strongest relation occurs when the film adopts the identical crystal lattice spacing of the substrate in the two dimensions of the film/substrate interface. This type of thin film growth is known as epitaxy. Epitaxial films are characterized by their coherency with the substrate meaning that corresponding atomic planes and lines are continuous across the film/substrate interface.

Epitaxial growth can occur even if the film and substrate do not have the same lattice parameters. The misfit between the two lattice parameters is overcome by straining the lattice of the film so it adopts the lattice of the substrate. The misfit strain is defined by the difference between the lattice parameters of the substrate and the film, normalized by that of the substrate (u_m=(b-a)/b). It is important to note at what temperature the misfit strain is being reported. The two most common temperatures to define the misfit strain are at room temperature and the temperature of the film's growth. The misfit strain at the growth temperature of the film will determine the initial misfit strain in the film when it is in the paraelectric state and is important for the formation of misfit dislocations. The misfit dislocation at room temperature is important since this strain is responsible for the domain structure of the film.

The strain energy in the film increases linearly with thickness. There is a limit to the amount of misfit strain that can be accommodated by the film. When the strain in the film

becomes too large the film will relax and coherency with the substrate is partially or completely lost. Relaxation of the film can occur through a variety of mechanisms. The two most important mechanisms for this paper are relaxation through dislocation generation and domain formation, the formation of differently oriented regions in the crystal.

As explained above the difference between an epitaxial film and a free film is that the former is strained so the lattice parameter of the film matches the lattice parameter of substrate. Coherency is maintained between the film and substrate at the expense of strain in the film. This strain is known as misfit strain [2]. In addition to misfit strain there are two more sources of strain; thermal strain and transformational strain. Thermal strain is caused by the substrate and film having different thermal expansion coefficients. Ferroelectric films are grown at high temperatures above T_c. As the film cools, the film and substrate contract by different amounts, creating strain in the film [4]. Transformational strain occurs when the film is cooled below T_c. At this point the elongation of the unit cell occurs, adding additional strain in the film [4].

2.2. Ferroelectricity:

A ferroelectric crystal is characterized by having a spontaneous polarization in the absence of an electric field below a transition temperature T_c. Another requirement of ferroelectricity is that the spontaneous polarization must be reversible when subjected to an external electric field. A plot of polarization versus electric field will give rise to a characteristic hysteresis loop seen in Figure 1. There are several mechanisms that cause ferroelectricity in a material. In $PbTiO_3$ the spontaneous polarization is the result of a shift in the centrosymmetric position of the atoms in unit cell of the crystal. The atomic shift is very small, on the order of 0.1Å, and is usually coupled with an elongation of the unit cell along the polar axis of the crystal [5].

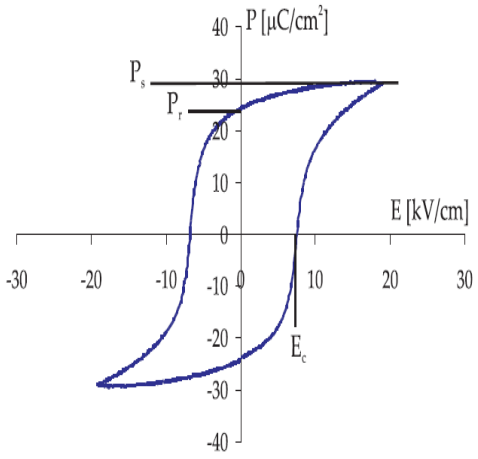

Figure 1. Ferroelectric hysteresis loop showing the saturation polarization (P_s), remnant polarization (P_r), and coercive field (E_c)

Whether or not a ferroelectric distortion will occur in a ABO_3 perovskite depends on the balance of two forces; short range repulsions and long range coulomb interactions. The short range repulsions favor the cubic paraelectric state while the long range coulomb interactions favor the ferroelectric state. The strength of the short range repulsions are weakened by hybridization between the B cation and the oxygen [6]. Hybridization will occur more easily if the B cation's lowest unoccupied states are d states. As a result most ferroelectric perovskites will have B cations that fulfill this requirement such as Ti^{4+}, Zr^{4+} and Nb^{5+}. The hybridization between these cations and the oxygen is strong enough to weaken the short range repulsion so that the ferroelectric distortion is favorable.

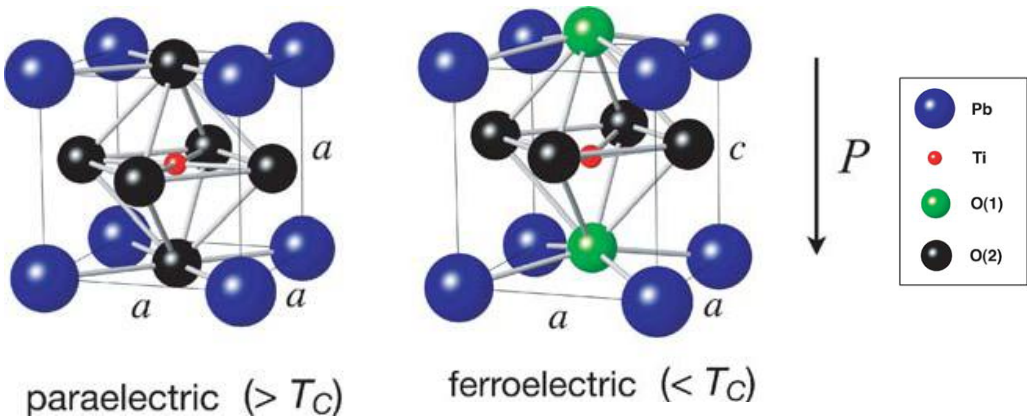

igure 2. Perovskite structure of $PbTiO_3$ above and below Tc showing the lattice distortions giving rise to a spontaneous dipole [5].

Understanding why a ferroelectric distortion is favorable in $PbTiO_3$ is seen by examining the calculated density of states for $PbTiO_3$ with and without a ferroelectric distortion which is shown in Figure 3 [6]. The top image shows the total density of states while the bottom two show the partial density of states from the Ti 3d (middle graph) and Pb 6s (bottom graph). It is clear from the total density of states that a ferroelectric distortion results in a shift in the density of states to slightly lower energies. The sum of the band eigenvalues is one term of the total energy, so a shift to lower eigenvalues means a smaller sum which represents a lower energy. As a result, the ferroelectric distortion is more stable

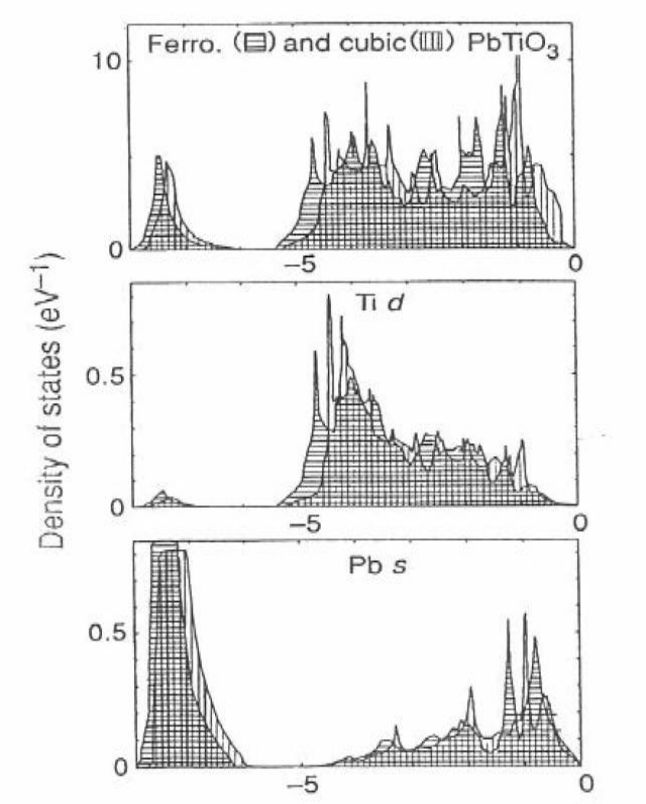

than the cubic structure.

Figure 3. Density of states vs. Energy (eV). The top graph represents the total density of states for the cubic and ferroelectric distortion. The middle and bottom graph represent the partial density of states for regions around the Ti with d character and Pb with s character respectively [6].

The reason the ferroelectric state is more stable than the cubic structure is understood by examining the partial density of states for the Ti 3d and Pb 6s. The energy of the oxygen 2p valence bands range from 0-~ -5.5 eV. There is large overlap for both the Ti 3d and the Pb 6s partial density of states with the energy regime for the oxygen 2p valence band meaning that there is significant hybridization taking place. This overlap also increases for the ferroelectric structure which allows for more hybridization making the ferroelectric distortion energetically favorable.

2.3 Ferroelectric Domains:

For a tetragonal ferroelectric film on a cubic substrate three different domain orientations are possible. A domain in which the c axis of the tetragonal film is aligned normal to the film/substrate interface is known as a *c* domain [7]. Similarly a domain in which the c axis of the tetragonal film is aligned parallel to the film/substrate interface is known as an *a* domain [7]. An *a* domain can have two different orientations a_1 or a_2, the difference being one is rotated 90° from the other [2]. The three domain orientations for a tetragonal film on a cubic lattice are schematically depicted in Figure 4 [7].

The spontaneous polarization of a ferroelectric crystal in the absence of an electric field is oriented in various directions. Regions of the crystal in which the spontaneous polarization is oriented in the same direction are known as ferroelectric domains. The different domains are separated by domain walls [2]. Domain walls are characterized by the approximate angle by which the polarization rotates between the two domains [3]. In epitaxial tetragonal ferroelectric thin films 180° and 90° domain walls are present. Since polarization also causes an elongation of the unit cell, a 90° rotation of the polarization must be accompanied by a rotation in the strain, or elongation, across the domain wall [5]. As a

result the 90° domain wall is ferroelectric and ferroelastic. A 180° domain does not have a rotation of the strain across the wall and is only ferroelectric in character [5].

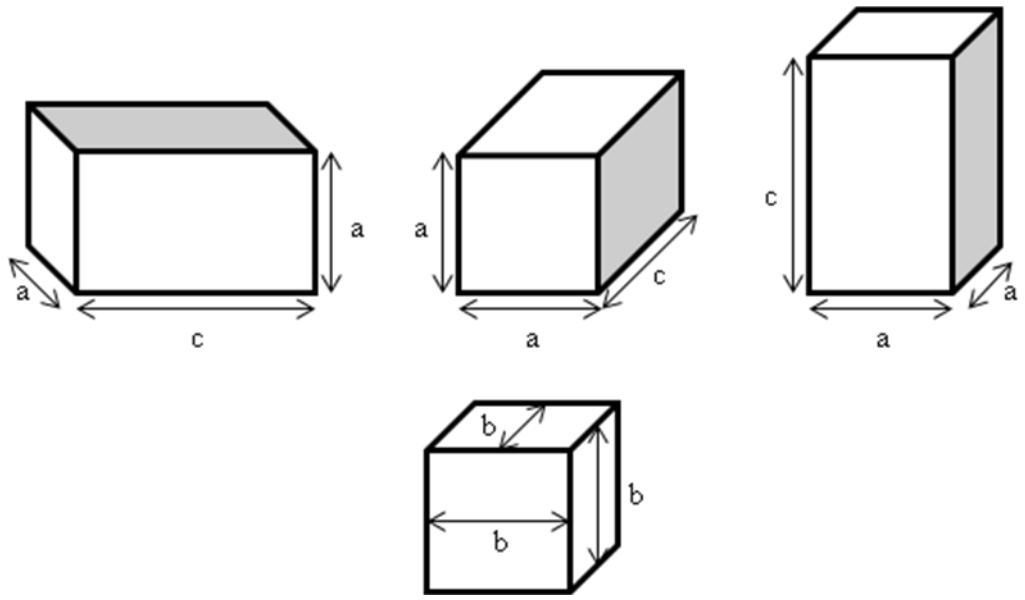

Figure 4. Domain orientations of an epitaxial tetragonal ferroelectric with lattice constants a and c on the [001] face of a cubic substrate with lattice constant b. From left to right a_1 domain, a_2 domain, c domain

Domain structures occur to minimize the strain and electrostatic energy of the film [7]. Strain in the film is relaxed by the formation of 90° ferroelastic domains. Since 180° domain walls are not ferroelastic, strain relaxation cannot take place in this way [2]. 180° domain structures form to decrease the depolarizing field, which is large for thin films. The depolarizing field is caused by having two interfaces with opposite charge creating an electric field. 180° domains alternate the charge on each interface preventing completely charged surfaces minimizing the depolarizing field. In addition to domain formation, strain relaxation can occur by the formation of misfit dislocation

2.4. Misfit Dislocations:

For sufficiently thin epitaxial films coherency is maintained between the substrate and the film at the expense of strain in the film. The strain in the film increases linearly with

thickness and at a critical thickness it becomes favorable for strain relaxation to occur and misfit dislocations will form [8]. The introduction of misfit dislocations into the film partially accommodates the lattice misfit and reduces the strain. The strain is relieved by edge-like components of the burgers vector that lie parallel with the interracial plane. Strain relaxation by misfit dislocations is especially important above Tc. At these temperatures strain cannot be relieved by domain formation and misfit dislocations are the only strain relaxation mechanism.

An equilibrium theory has been developed to quantitatively describe the critical thickness for misfit dislocation generation and to determine the misfit dislocation density in a partially relaxed film. This theory, developed by Matthews and Blakeslee, models the energy per unit area of a film that is partially relaxed by misfit dislocations as the sum of the energy per unit area corresponding to the misfit strain and the dislocation array, Equation 1 [9]. In the equation ε_m is the misfit strain, ρ_{md} is the misfit dislocation density (number of dislocation per unit length), β is the angle between the Burgers vector and the dislocation line, *h* is the film thickness, ν is Poisson's ratio, and α is a numerical constant with a value around 4.

$$U^{tot} = \frac{hE}{(1-\nu)}(\varepsilon_m - \rho_{md}|b|\cos(\lambda))^2 + \rho_{md}\frac{E|b|^2}{4\pi(1+\nu)}\left(\frac{1-\nu\cos(\beta)^2}{1-\nu}\right)ln\left(\frac{\alpha h}{|b|}\right)$$

Equation 1.

For a given thickness misfit dislocations will form if an increase in ρ_m results in a decrease in the total energy. Mathematically the critical thickness for misfit dislocation generation is determined by $(\partial U_{tot}/\partial p_{md})_{pmd=0}=0$, when the increase in the density of dislocations causes a decrease in the total energy. This gives the Matthews and Blakeslee criteria for the initial introduction of misfit dislocations which is shown in Equation 2, [9].

The critical thickness for misfit dislocation generation is inversely proportional to the misfit strain.

$$h_c = \frac{|b|}{8\pi\varepsilon_m \cos(\lambda)}\left(\frac{1-\nu\cos(\beta)^2}{1+\nu}\right) ln\left(\frac{4h_c}{|b|}\right)$$

Equation 2.

This model provides a reasonably good description of relaxation by misfit dislocations. However, being a thermodynamic theory it does not take into account any kinetic considerations such as nucleation, motion, and multiplication of dislocations in epitaxial films. As a result, this theory underestimates the critical thickness in many cases. Experimental studies have shown that introduction of misfit dislocations can occur at much larger thicknesses. Other models such as that of People and Bean, are then used to explain misfit dislocation formation [10]. Unlike the Matthews and Blakeslee model, People and Bean assumed that dislocation must first nucleate. As a result the energy balance become a competition between the misfit strain and the energy required to nucleate a dislocation. The inclusion nucleation energy produces critical thicknesses that are more consistent with experimentally obtained values for the critical thickness.

2.5. 90° Domains:

Below the transition temperature of the film strain relaxation can occur by the formation of 90° domains. Adopting a periodic c/a/c/a domain structure allows the film lattice to relax while still maintaining partial coherency with the substrate over the domain periodicity, a schematic of this is shown in Figure 5.

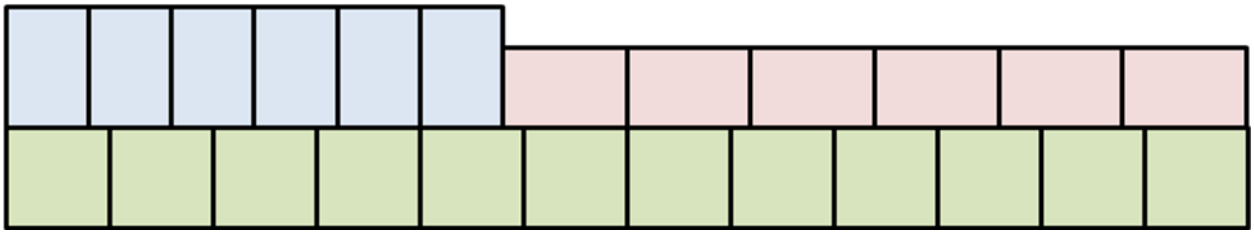

Figure 5. Schematic of 90° domain structure showing misfit relaxation while still maintaining long range coherency with the substrate

Although this model provides a good qualitative explanation of how coherency with the substrate is achieved by 90° domains, it does not address how the different crystal orientations are joined at the interface. This is accomplished by twining along the (101) plane [2]. Twining allows for coherency across the domain wall, thereby lowering the strain energy of associated with domain wall formation. Due to the tetragonality of the film, twinning will result in a slight deviation of the rotation of the polarization from 90° across the domain wall. The deviation is completely determined by the ratio of a/c [11]. The small deviation causes a domain tilt perpendicular to the film substrate interface which must be accommodated by the film. A schematic of 90° domains formed by twining for both a cubic and tetragonal crystal is shown in Figure 6.

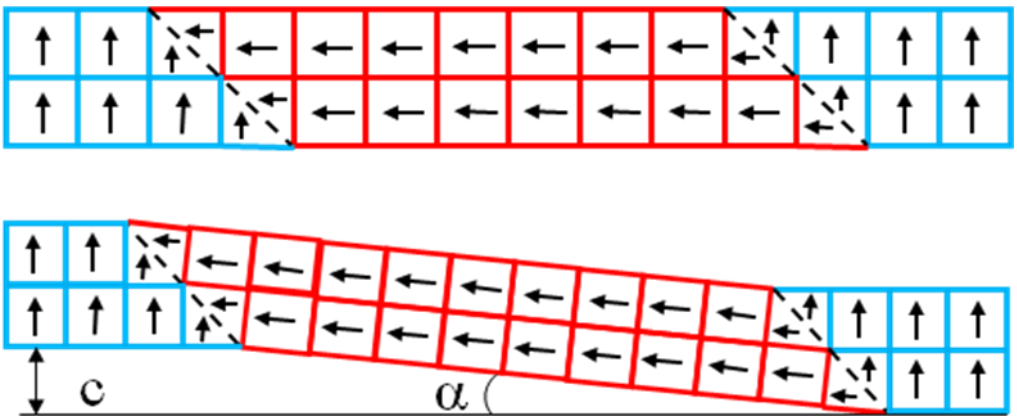

Figure 6. Schematic of 90° domain structures with twining along (101) for a cubic (top) and tetragonal (bottom) unit cell

Another consequence of the domain tilt is that it can limit the width of the *a* domains. To maintain lateral coherency between two adjacent c domains the rows of atoms in two consecutive c domains must be connected by an *a* domain. For this to happen the *a* domain must have the appropriate width so the domain tilt will result in an out of plane deviation equal to the c lattice parameter of the film. Therefore the width of the *a* domains is constant and determined by c/sin(α) [11].

The relationship between the domain periodicity and the film thickness is determined theoretically by examining the free energy expression for the film. The free energy associated with 90° domains is the sum of two components, the energy of the domains themselves and the energy of the domains walls. The energy of the domains scale with the domain size while the energy of the domain walls depends on the area of the wall (determined by the thickness) and the total number of walls (inversely proportional to the domain periodicity). Using U and γ as proportionality constants, the free energy expression is $F= Uw+ \gamma(d/w)$ where w is the domain size and d is the film thickness [12]. The equilibrium domain periodicity is calculated under equilibrium conditions, $dF/dw=0$. The result is the domain periodicity is proportional to the square root of the film thickness.

The free energy expression above is applicable for any ferroic material. This approach was initially developed by Kittel for ferromagnetic materials [13]. Mitsui and Furuichi then applied this technique to ferroelectric (180°) domains [14]. Finally Roytburd adapted this approach for epitaxial ferroelastic (90°) domains [15]. In the case of 90° domains the proportionality between the square root of the film thickness and the domain periodicity depends of the shear modulus G and the strains of the short and long lattice parameters of the film, s_a and s_c. This equation is shown in Equation 3 [12]. This approach is justified as long

as the domain structure is dense, when the domain periodicity is much smaller than the film thickness.

$$w^2 = \frac{4\pi 8^3}{8.42}\frac{\gamma d}{G(s_a - s_c)^2}$$

Equation 4.

This theory does not address strain relaxation from misfit dislocations. To incorporate misfit dislocations, an effective substrate lattice parameter was introduced. This parameter changed the misfit strain in the film used in the theory to accurately reflect strain relaxation that occurred from misfit dislocation [8]. Even using an effective substrate lattice parameter, the theory still limited to the case of dense domain structures.

Other more rigors theories have been developed to explain the domain periodicity for domains similar in size to the film thickness. Approaches that have been used include; modeling the mechanical stress sources located on domain boundaries and the film/substrate interface by continuously distributed fictitious dislocations [16], and treating the free energy of the film as an expression of the order parameter which is then minimized to determine the equilibrium domain structure [17].

3. Experimental

4.1. Pulsed Laser Deposition:

The thin films examined in this research are grown using the pulsed laser deposition technique (PLD). PLD is a physical vapor deposition technique (PVD). Like other PVD techniques, such as molecular beam epitaxy and plasma sputtering, a physical process is used to deposit the material onto a substrate. As in any PVD process, chemical reactions do not take place.. In PLD a pulsed laser provides the energy needed to create a plasma.

Since the discovery of lasers scientists, have been interested in using lasers as an energy source for thin film growth. Initial PLD experiments were carried out in the 1960's [18]. Limited research continued in the 1970's and 80's. Throughout this period PLD remained little more than a scientific curiosity and was not considered a serious technique for thin film growth. However, this changed dramatically with the discovery of high temperature superconductors in the late 1980's. These new superconductors were complex oxides and PLD proved to be a fast, reproducible way to grow thin films of these superconductive oxides [19]. As a result, interest in PLD exploded and over the last 20 years PLD has become a common technique for growing thin films of many different materials including metals, insulators, semiconductors, polymers, and even biological material.

A schematic of the PLD process is shown in Figure 7 [18]. PLD starts by focusing a pulsed laser onto a target of material that is to be deposited. If the laser pulse has a high enough energy density the target material will ablate forming a plasma just in front of the target. Ablation of the target takes place during the initial portion of the laser pulse. The ablated material will continue to absorb energy for the remainder of the laser pulse. This energy absorption will increase the pressure and temperature of the material resulting in partial ionization. The increased pressure of the vapor causes an expansion away from the target creating what is known as a plasma plume [18]. It is this plume that provides the material flux needed for film growth. Parallel to the target is the substrate upon which the film is grown. When the plasma reaches the substrate, a phase transition occurs and the material is deposited on the substrate surface.

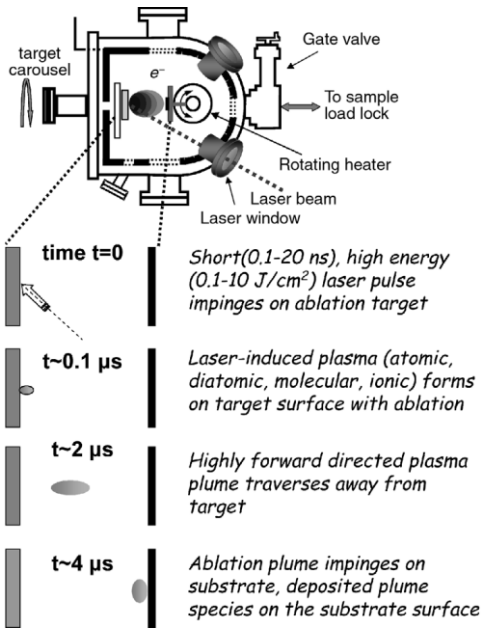

Figure 7. Schematic of PLD process chamber and overview of deposition process [18]

The biggest advantage of PLD over other thin film deposition techniques for the growth of complex oxide thin films is the stoichiometric transfer of material from the target to the substrate [18]. Stoichiometric transfer is achieved through the non-equilibrium nature of the ablation process. If the energy density of the laser pulse on the target was not large enough for ablation, evaporation of the target would occur. In this scenario the material flux of each constituent in the target is different and determined by its vapor pressure.

Another advantage of PLD is the ability to control the kinetic energy of the ablated species [18]. This control is used to modify the growth of the thin film and is achieved through the introduction of a background gas into the process chamber. Collisions between the ablated species and the background gas decrease the kinetic energy of the ablated species. Two parameters of the background gas are important in determining the kinetic energy of the ablated particles; the pressure and the mass. As a result for a given background gas the kinetic energy of the ablated material can be varied from high energy at low pressure to low energy at high pressure.

The major disadvantage of PLD is that it cannot be easily scaled up. Expansion of the plasma plume is directed very strongly away from the target and as a result the thickness distribution is non-uniform. For typical PLD depositions uniform thickness can only be achieved over few centimeters. Using PLD to grow large area films requires the plasma plume to be rastered over the substrate which introduces complications in the growth process. Although such systems already exist, from a commercial point of view PLD is not a very attractive growth technique due to the area restrictions of the film growth.

3.2. Growth Kinetics:

In order to observe the small topographical changes between a and *c* domains using AFM (the aim of this project), the ferroelectric film needs to be as flat as possible. Growth of atomically flat thin films requires control over the growth mode. Epitaxial growth of thin film oxides can occur through several different growth modes. Understanding the mechanisms that affect the growth mode of the film is therefore necessary to create flat films. Reflection high energy electron diffraction (RHEED) is used to monitor the film growth *in situ* and is used to determine the growth mode of the film.

Two independent processes are important in epitaxial growth on a flat surface. These processes are nucleation and growth. Nucleation causes the formation of islands while growth causes lateral movement of these islands [19].

In PLD material is only transferred from the target to the substrate during a laser pulse. This unique feature of PLD will affect the nucleation and growth processes. The short laser pulse means that the random deposition of atoms onto the substrate is separated in time from nucleation and growth. To illustrate this feature, consider the time scale needed for the deposited atoms to rearrange on the substrate surface to nucleate and grow. This time scale is defined using the mean diffusion time of the deposited atoms (t_D) given in Equation 4 [20],

where ν is the attempt frequency, E_a is the activation energy and k_b is Boltzman's constant. For many deposition conditions, t_D is longer than the pulse duration. As a result PLD growth is viewed as a two step process. First atoms are randomly deposited on the surface followed by a relatively long time interval where no deposition takes place. During the interval after the laser pulse, the deposited atoms rearrange on the surface where nucleation and growth will occur.

$$t_d = \nu^{-1} \exp\left(\frac{E_a}{k_b T}\right)$$

Equation 5.

Under typical PLD growth parameters film growth does not occur at thermodynamic equilibrium [20]. As a result, a number of kinetic parameters will determine the growth mode. These parameters include the surface diffusion coefficient (D_s), the sticking probability of a deposited atom arriving at a step surface, and the additional energy barrier for a deposited atom to descend a single step edge (Es).

The surface diffusion coefficient determines how far a deposited atom can travel on the surface which is expressed by the surface diffusion length (l_D). If l_D is much larger than the step surface width then the deposited atoms are able to diffuse to the steps edges where they are incorporated into the film. As a result nucleation does not occur on the step surface. As more atoms arrive at the step edges the steps will grow and "move" across the surface. This growth mode is known as step flow growth and is shown schematically in Figure 7d [20].

If l_D is not larger than the step width then nucleation will occur on the step surface. Nucleation will take place until a saturation density is achieved. At this nucleation density it becomes more probable for a deposited atom to join an existing nucleus instead of creating a

new nucleus. At this point existing nuclei will start to grow. In this case the growth mode is determined by E_s.

If there is a small energy barrier for an atom to descend a step (small E_s) then diffusing atoms that arrive at the edge of a growing island are able to descend and fill in the space between the islands. This will result in layer by layer growth, shown in Figure 8a [20]. For ideal layer by layer growth nucleation of the next layer should not occur until the previous layer is completely filled.

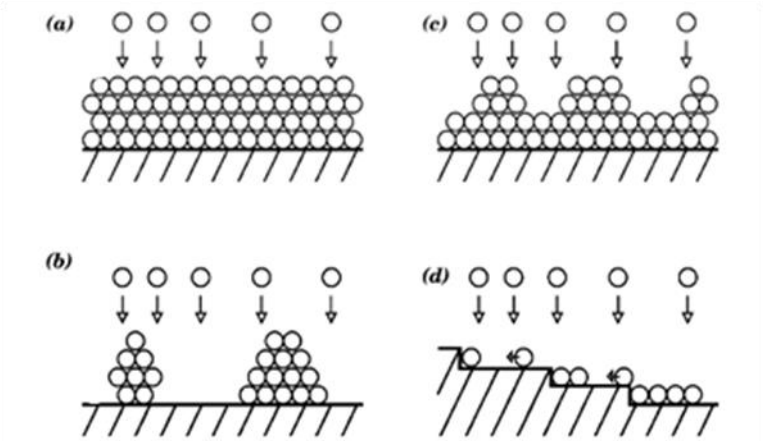

Figure 8. Film growth modes (a) layer by layer, (c) island, (d) step flow [20]

If there is a large energy barrier for an atom to descend a step (Large E_s) then deposited atoms will not descend off the islands. As a result further nucleation will occur on top of the islands and multilayer growth occurs, Figure 7c. [20] For the growth of real films under non-equilibrium conditions were l_d is smaller than the step width, growth will take place as a mixture of layer by layer and multilayer growth.

The magnitude of D_s, and subsequently l_D, Equation 6 [20], is determined by several intrinsic parameters such as the activation energy for diffusion (E_a), the attempt frequency (v), and the jump distance (a). However, D_s also depends on the temperature. This allows control of the growth mode.

$$D_s = \nu a^2 \exp\left(\frac{E_a}{K_b T}\right)$$

Equation 6

3.3. *In situ* growth monitoring using RHEED:

RHEED is an ideal tool for monitoring the growth of thin films using PLD. Information about the film surface is provided by the diffraction of electrons from the periodic arrangement of surface atoms. RHEED has been around for a long time. However, it wasn't until the development of high pressure RHEED in 1997 that this technique could be used in PLD to monitor the surface of growing films in real time [21].

A schematic of a typical RHEED setup is shown in Figure 9 [21]. A monoenergetic beam of electrons strikes the surface at a grazing incidence. These electrons are provided by an electron gun. The diffraction pattern is displayed on a phosphorus screen and this information is displayed in real time. Both the electron gun and the phosphorus screen must be far enough away from the substrate and target to avoid interactions with the PLD process.

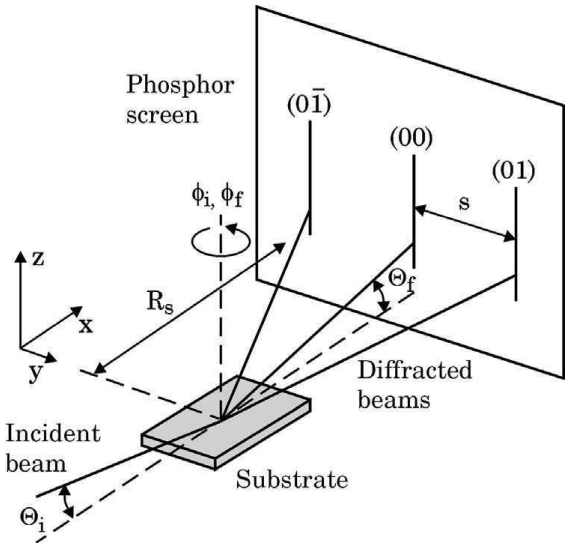

Figure 9. Schematic of RHEED set-up showing the major elements involved in the technique [21]

Typical electron energies range form 10-50 KeV which result in an electron wavelength of ~.05-.1 A [21]. The electron wavelength for the highest energy electrons typically is an order of magnitude smaller than the thickness of a single monolayer. At grazing incidence the penetration depth of the electrons is only a few monolayers. This surface sensitivity is what makes RHEED such an ideal candidate to monitor thin film growth.

The diffraction pattern collected on the phosphorus screen contains a great deal of information about the film being grown. The distance between diffraction spots is used to calculate the lattice parameters of the film. The symmetry of the spots and their behavior upon rotation of the film provides information on the morphology of the film surface [22]. Most important for thin film growth monitoring, the growth mode and layer thickness is inferred by the behavior of the intensity of the diffraction spots as a function of time. Schematics of different surface features with the corresponding characteristic RHEED diffraction patterns are shown in Figure 11-1 [23].

To understand how the intensity oscillations can provide information on the growth mode and film thickness it is useful to use the Ewald sphere construction as a geometrical representation of the diffraction process. This representation is depicted in Figure 10 [22]. The reciprocal lattice of a 2D surface is a lattice of infinitely thin rods. A diffraction spot will occur whenever the Ewald sphere intersects a rod. The radius of the Ewald sphere is determined by the energy of the electrons. From this geometry it is clear the diffraction spots will lie on concentric circles which are known as Laue circles. The energy of the electrons typically used for RHEED will result in large Ewald spheres compared to the spacing of the reciprocal lattice rods. As a result only a few diffraction spots are obtained.

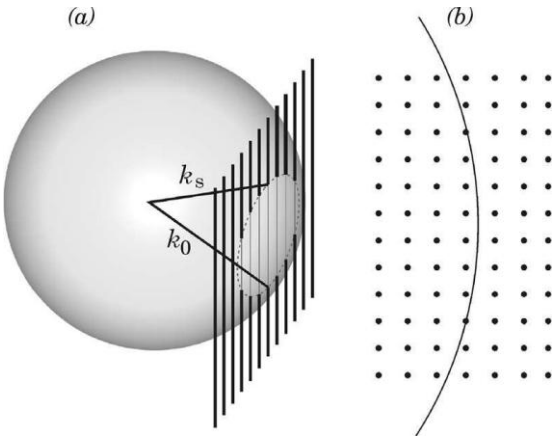

Figure 10. Ewald sphere construction in (a) three dimensions and (b) a section of the horizontal z=0 plane [21]

Real epitaxial films do not have perfect 2D surfaces. Instead real films can have quasi 2D surfaces which consist of steps with one unit cell height. Each step will cause diffuse scattering of the RHEED electrons decreasing the intensity of the diffraction spots. As a result, the more steps the weaker the intensity of the diffractions spots. During layer by layer growth nuclei with a height of one unit cell will form on the surface of the film. The steps formed by each nuclei will decrease the intensity of the RHEED pattern. This decrease in intensity will continue as the more nuclei form and grow. The layer will fill in as nuclei grow together. This results in decrease in the number of steps on the surface causing the intensity of the diffraction spots to increase. Finally when the layer is complete the intensity of the spots will return to its initial value. Each intensity oscillation during growth will correspond to the addition of one monolayer to the film thickness. A schematic of the intensity oscillations for different growth modes is shown in Figure 11-2 [23].

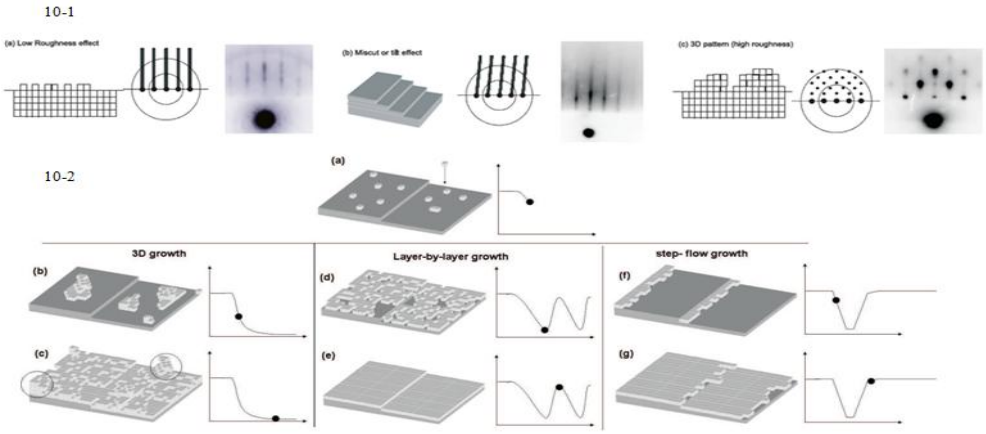

Figure 11. 11.1-Schematic of surface feature and the effect on the RHEED diffraction pattern, (a) low roughness, (b) miscut, (c) 3D growth. 11.2- Typical modes observed in thin film and their corresponding evolutions of the RHEED intensity. (a) Arrival of species at the substrate. (b)-(c) 3D island growth. (d)-(e) 2D layer-by-layer growth. (f)-(g) 2D step-flow [23]

.

3.4. Reciprocal Space Maps:

Reciprocal Space Mapping (RSM) is an X-ray diffraction technique in which an area of reciprocal space is mapped instead of just a single line scan. This technique is performed by taking 2θ-ω scans for varying ω angles. A schematic of how this technique is preformed is shown in Figure 12 [24]. RSMs provided a lot of information about the film. Tilted growth and twining in the film are observed in a RSM. Twining is observed in reciprocal space as a lattice which is tilted from a reference lattice. In this way the tilted *a* domains are easily seen in a RSM.

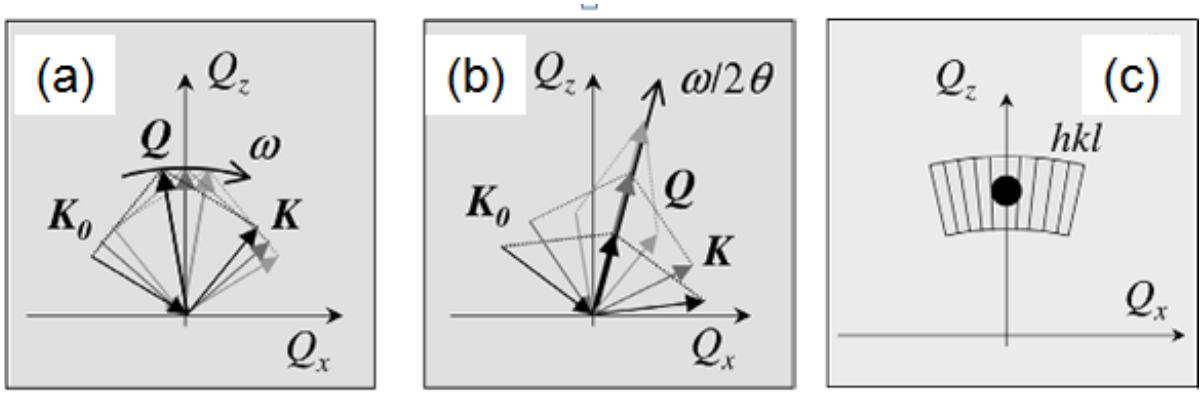

Figure 12 RSM schematic, (a) ω scan, (b) 2θ-ω, (c) reciprocal space map using 2θ-ω scans for various ω angles [24]

3.5. Atomic Force Microscopy:

Atomic Force Microscopy (AFM) is a scanning probe technique which uses a micrometer cantilever to trace the surface morphology. A schematic of a typical AFM set up is shown in Figure 12. In this technique a micrometer cantilever with a sharp tip of approximately 10 nm is brought close to the surface of a material. Interactions between the sample surface and the tip will bend the cantilever. These deflections are detected by a laser beam which is bounced off the cantilever on to an array of photodiodes. Once the tip is brought into close proximity with the surface the height of the tip is adjusted to maintain a constant deflection of the cantilever as it is passed over the surface. The changes in the tip height required are recorded and in this way a trace of the surface morphology is recorded.

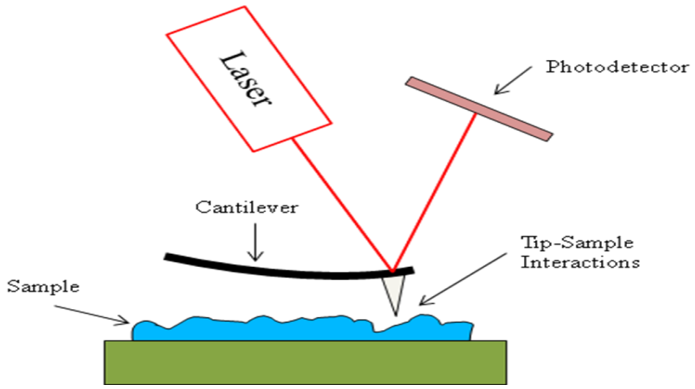

Figure 13. Schematic of AFM set-up showing the major elements involved in this technique

In this paper tapping mode AFM has been used to obtain images of the surface morphology. In this case the cantilever is not stationary but instead oscillated a frequency close to the resonant frequency. Interactions between the tip and the surface will cause deviations in the amplitude of the cantilever. In this case the height of the cantilever is adjusted to maintain constant oscillation amplitude. The main advantage of this technique is that the tip will spend less time in contact with the sample and as a result the method is much gentler on the sample and the tip.

3.6. Piezoresponse Force Microscopy:

Currently there are several scanning probe microscope (SPM) techniques that are used to image ferroelectric domains. In these techniques contrast is achieved by examining the difference in mechanical, structural, electromechanical, dielectric, or piezoelectric properties of differently oriented ferroelectric domains [25]. The most widely used of these techniques is piezoresponse force microscopy (PFM). This technique is based upon the reverse piezoelectric effect which describes the linear relationship between the applied electric field and the spontaneous stress in a piezoelectric material ($x_{ij}=d_{ijk}E_k$) [26]. All ferroelectric materials are also piezoelectric and will change dimensions in response to an electric field. However, in a ferroelectric the piezoelectric coefficient will depend on the spontaneous polarization and for the case of a tetragonal ferroelectric $d_{im}=\varepsilon_{ij}Q_{mjk}P_{sk}$, where Q is the electrostrictive coefficient [27].

PFM is preformed on a ferroelectric film sandwiched between a bottom electrode and a conducting SPM tip. The conducting SPM tip serves as a movable top electrode allowing localized probing of the ferroelectric domain structure. To understand how PFM works it is important to consider two cases; when the spontaneous polarization is oriented out of plane and when the spontaneous polarization is oriented in plane.

First consider the case of two ferroelectric domains having opposite polarization orientation perpendicular to the film/substrate interface as depicted in Figure 14. When a voltage is applied to the tip an electric field is generated in the sample resulting in a deformation of the ferroelectric. Domains with polarization parallel to the electric field will expand while domains with polarization anti-parallel to the electric field will contract. The deformation depends linearly on the piezoelectric coefficient. For a tetragonal ferroelectric the deformation is expressed by $\Delta z=-d_{33}^{*}V$, $d_{33}^{*}=d_{33}$ for $P_z>0$ and $d_{33}^{*}=-d_{33}$ for $P_z<0$ [26].

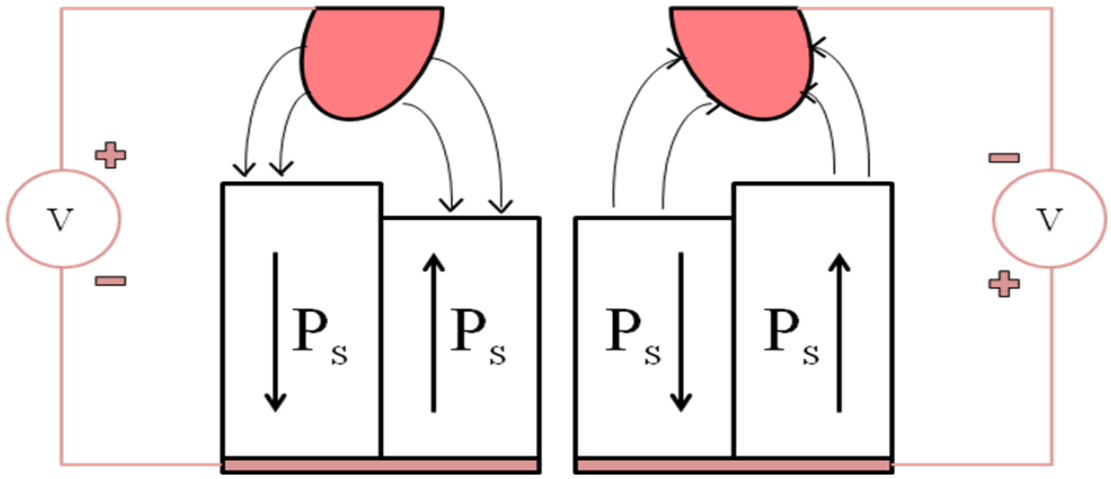

Figure 14. Detection of out of plane polarization using PFM for positive and negative applied voltage

Using this formula it is easy to calculate the expected deformation of the ferroelectric. A ferroelectric with d_{33}=50pm/V subjected to an applied voltage of 4 V will have a deformation of 0.2nm. This deformation is near the limit of what a typical SPM can detect. In addition, other surface features will obscure the piezoresponse of the ferroelectric making its detection very difficult.

Detection of the piezoresponce is achieved by applying an AC voltage to the tip. In this case the applied voltage is $V=V_{ac}\sin(wt)$. The oscillating voltage will result in periodic expansion and contraction of the domains. Now the change in deformation of the ferroelectric is $\Delta z(t)=-d_{33}{}^{*}V_{AC}\sin(\omega t)$ [26]. Now the difference between the two domains is that they vibrate out of phase from one another. Although the magnitude of these vibrations is still very small they can be detected using a lock-in technique.

Now consider ferroelectric domains with polarization parallel to the film/substrate interface. Now the polarization is perpendicular to the applied electric field and there is piezoelectric deformation in the direction of the field. However, shear strains are present causing deformations along the polarization directions. Although there is no change in the

surface topography these deformations are still detected by the tip. Lateral deformation will cause torsion of the PFM tip as the ferroelectric deforms, show schematically in Figure 15. Now the deformation is expressed by $\Delta x=-d_{15}{}^{*}V$ [26]. For the same reason already mentioned imaging of in-plane domains is done using an AC voltage. An AC voltage will result in an oscillation of the deformation and domains with opposite polarization are out of phase from one another. It is important to note that deformations will take place in both in-plane directions. However, due to the cantilever geometry only deformations perpendicular to the long axis of the cantilever will result in torsion of the tip. The amplitude of the torsion motion of the cantilever is larger than that of the vertical motion and thus, the in-plane sensitivity is larger.

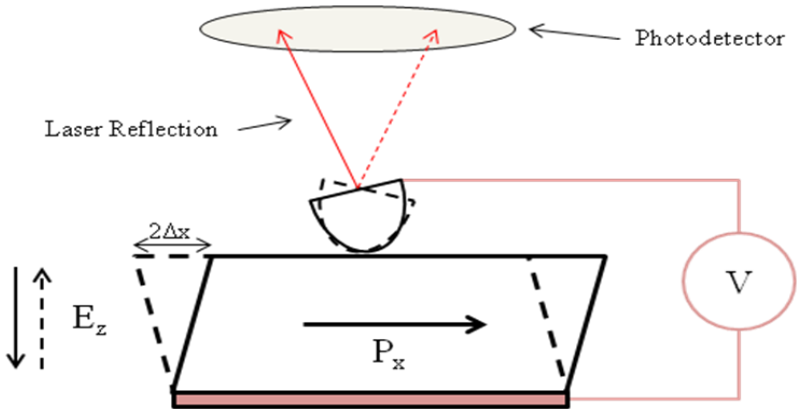

Figure 15. Schematic of detection of in plane polarization

4. Results

4.1. $DyScO_3$ Substrate:

$DyScO_3$ has been chosen as the substrate material due to its excellent lattice match with $PbTiO_3$. At room temperature the $PbTiO_3$/ $DyScO_3$ lattice misfit is approximately 1.4%. At this misfit strain the film is right at the theoretical border between the 180° and 90° domain structures, seen in Figure 16 [16]. Above T_c the lattice misfit is ~-.005%. The very small

hight temperature misfit will prevent the formation of misfit dislocation and strain relaxation will almost entirely take place through domain formation at Tc. Therefore, $PbTiO_3$ films grown on $DyScO_3$ is almost entirely defect free.

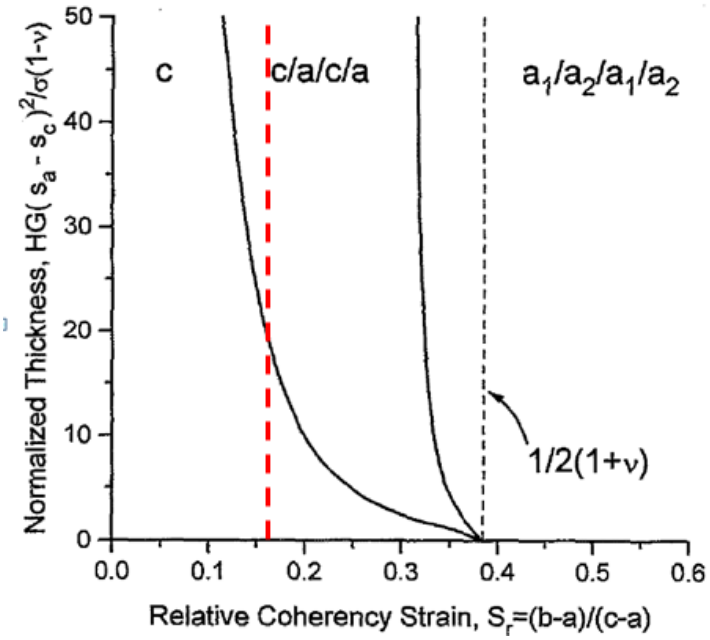

Figure 16. Relative Coherency strain vs Normalized film thickness for a tetragonal film on a cubic substrate. The dashed line represents the relative coherency strain for $PbTiO_3$ on $DyScO_3$ at room temperature. [16]

Atomically flat substrate surfaces are necessary for epitaxial growth and for a coherent film/substrate interface. A combination of mechanical cleaning and thermal treatment is used to obtain atomically flat $DyScO_3$ surfaces. Mechanical cleaning of the substrate surface was performed by placing the substrates in 30 minute ultrasonic baths of acetone by a 30 min ethanol bath. At this point the substrate is then cleaned by rubbing with optical tissue and ethanol. The substrate is then returned to 30 minute ultrasonic baths in acetone followed by ethanol. Following the mechanical cleaning the substrate is subjected to thermal treatment. The substrate is annealed for 24 hours at 1020° C. During heating and cooling a 200ml/min O_2 flow is applied.

The resulting surface is examined using AFM, shown in Figure 17. Flat steps with widths of approximately 95nm are clearly seen in the image. Taking a topographical profile across several of the steps reveals that the step height is approximately 4Å, which corresponds to the height of one unit cell of $DyScO_3$. Therefore the surface is atomically flat with single unit cell steps.

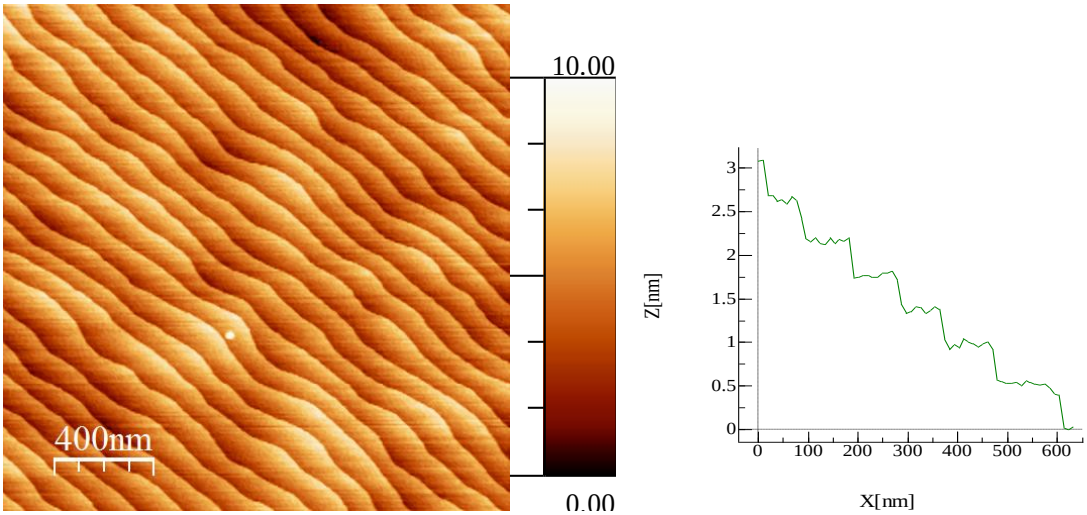

Figure 17. Left, AFM image of $DyScO_3$ surface after mechanical and thermal treatment (Z scale in angstroms). Right, line profile over several steps

5.2. $SrRuO_3$ Electrode:

Piezoresponce force microscopy requires a conductive electrode under the $PbTiO_3$ film. In these experiments $SrRuO_3$ is used as an electrode material. A 30nm $SrRuO_3$ film is grown using PLD at a growth temperature of 700° C. At this temperature the misfit strain between the film and the substrate is .4% which is small enough to ensure misfit dislocation will not form.

In order to grow an epitaxial ferroelectric film on the electrode it is important the the $SrRuO_3$ layer has a flat surface. The surface morphology of the $SrRuO_3$ films is shown in Figure 18. The films surface consists of two distinct features; steps and wedding cakes. The profile in Figure 18 reveals that the steps have an average width of 40nm and a height of

approximately 2Å which corresponds half of a $SrRuO_3$ unit cell. However, the steps that form the wedding cake structure have a height of approximately 4Å corresponding to a full unit cell. Although the $SrRuO_3$ electrode layer has shorter steps and the steps are broken up by wedding cake structures the surface is sufficiently flat and can be used to grow $PbTiO_3$ films. AFM images of the other 30nm $SrRuO_3$ electrodes are shown in Appendix A. In two cases a flat $SrRuO_3$ film is not obtained. This has been attributed to a dirty window on the PLD chamber that the laser must pass through which will cause contamination of the film and loss of control over laser energy.

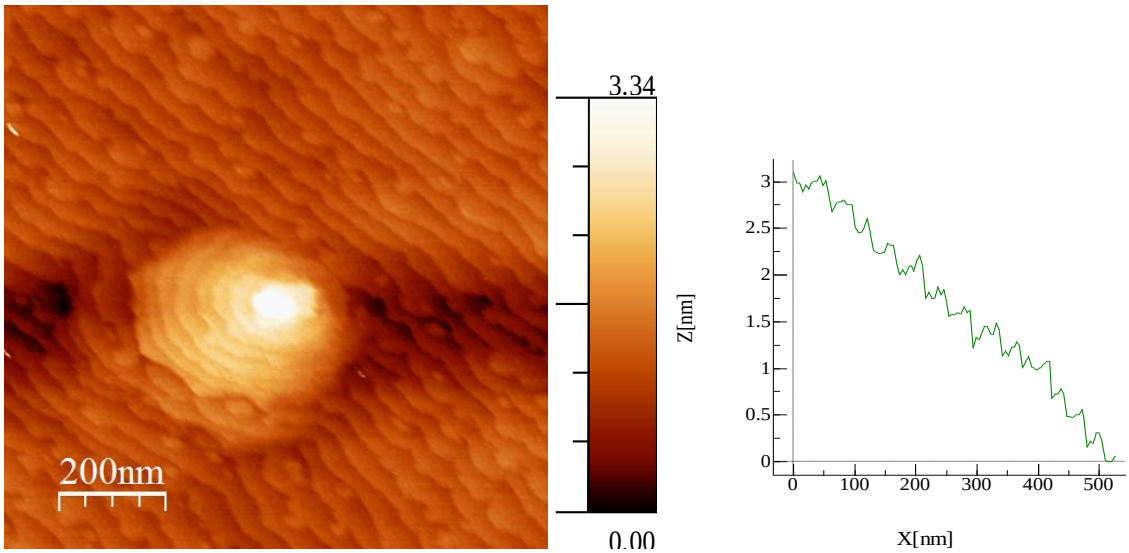

Figure 18. Left, AFM image of $SrRuO_3$ surface (z scale in nm). Right, profile across several steps

5.3. $PbTiO_3$ Films:

$PbTiO_3$ films are grown using PLD at a growth temperature of 570° C. Films of varying thickness from 24nm to 44nm are grown by varying the deposition time. To prevent any contamination of the electrode surface the samples were not removed from the PLD chamber before the growth of the $PbTiO_3$. After the deposition the films are cooled at a rate of 5°C/min to ensure that equilibrium domain structures will form when the film is cooled

through the transition temperature. The thickness of the $PbTiO_3$ films is determined using X-Ray reflectometery.

A 2θ-ω scan for one of the $PbTiO_3$ films is shown in Figure 19. The peaks corresponding to all three materials are clearly seen. The strongest peak corresponds to the $DyScO_3$ substrate. $SrRuO_3$ has a slightly smaller out of plane lattice parameter than the substrate and its peak is seen just to the right. Finally $PbTiO_3$ has a larger out of plane lattice parameter and its peak is therefore to the left of the substrate. 2θ-ω scans for all the films are shown in Appendix B.

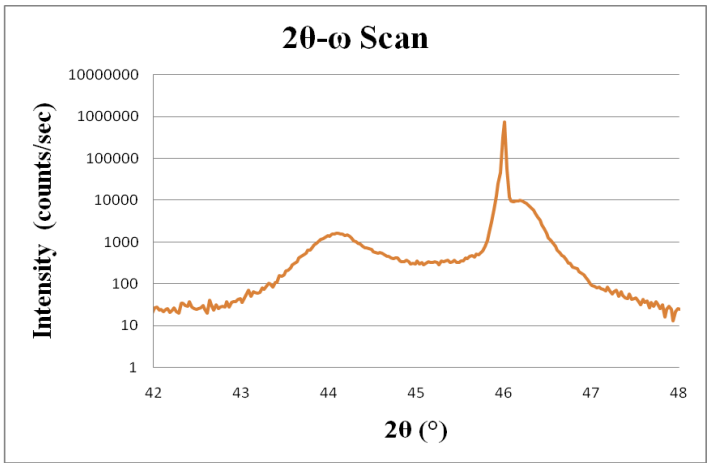

Figure 19. 2θ-ω scan around 002 peak for a 30.5 nm thick $PbTiO_3$ film on a 30nm thick $SrRuO_3$ electrode with a $DyScO_3$ substrate.

A reciprocal space map around the 002 peak is shown in Figure 20. The three peaks are seen corresponding to the $PbTiO_3$ film (bottom peak), the $DyScO_3$ substrate (middle peak), and the $SrRuO_3$ electrode (top peak). The three peaks are all centered around the k=0 axis. A striking feature about the RSM are the four wings extending out from the k=0 axis. These wings are the result of *a* domains present in the $PbTiO_3$ film meaning there is a 90° domain structure. The disinclination of the *a* domains from twinning means scattered intensity in reciprocal space from these regions of the ferroelectric are tilted with respect to the *c* domains producing intensity out of the k=0 axis.

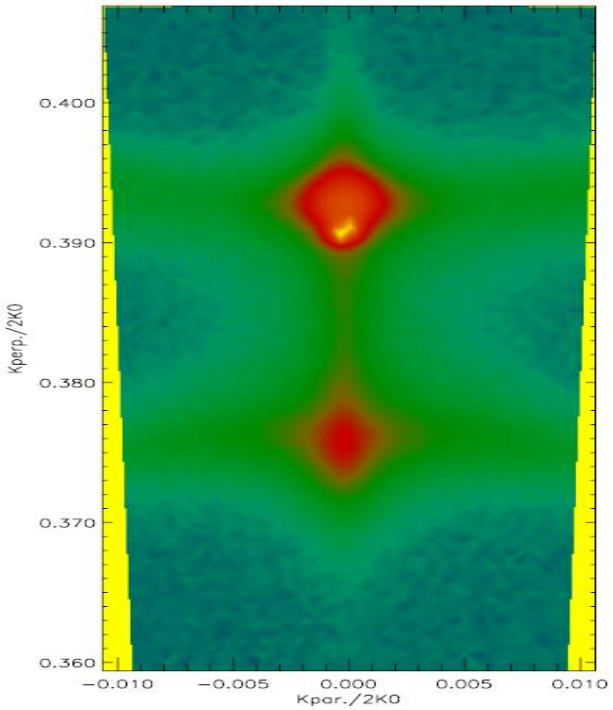

Figure 20. RSM around (002) peak showing the presence of a domains

The surface morphology of the $PbTiO_3$ film is investigated using AFM. A characteristic image is shown in Figure 21. In this image periodic narrow ridges are seen along the diagonals. This also confirms the presence of *a* domains in the film. These ridges are small and have only a slight out of plane deviation, both features which are characteristic of an *a* domain. AFM images of all the films are shown in Appendix C.

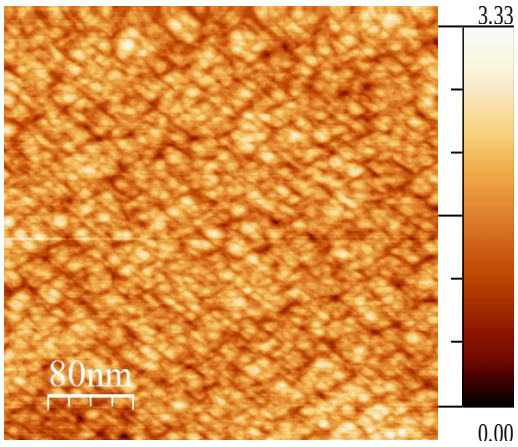

Figure 21. AFM image of $PbTiO_3$ films surface (z scale in nm)

Piezoresponse force microscopy is also used to image the ferroelectric domains. The amplitude of the out of plane peizoresponse is shown in Figure 22a compared to the surface morphology taken using AFM in Figure 22b. In the PFM image two regions having an opposite out of plane amplitude response are distinguishable. The regions of opposite response are quite large, especially when compared to the size of the ridges seen in the AFM image. It is clear that the PFM is not imaging the *a* domains but only the adjacent *c* domains. A possible reason for this could be due to a loss of spatial resolution due to the larger size of a conductive tip compared to a standard AFM tip. Additional out of plane PFM images are shown in Appendix D.

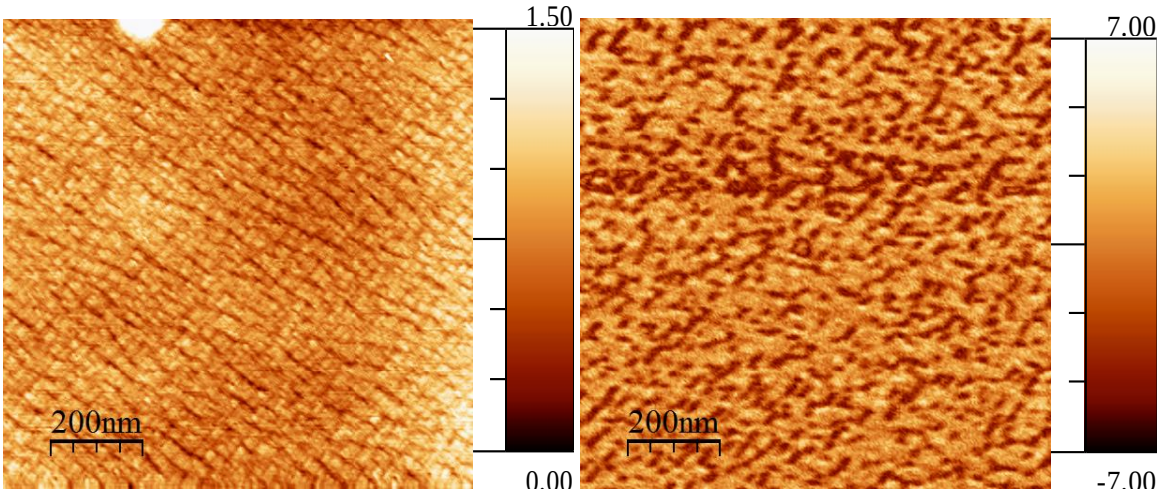

Figure 22. Left, AFM image of $PbTiO_3$ films surface (z scale in nm), Left, amplitude of out of plane PFM of same $PbTiO_3$ film (z scale in V)

The domain periodicity has been determined by analyzing the AFM images using a Fast Fourier Transform (FFT) technique. The steps of this process is shown in Figure 23 . The resulting FFT profiles show the intensities of different periodicities and several strong peaks are seen. The strongest peak is always present very close to the center and corresponds to a domain periodicity over 100 nm. This periodicity is the result of large surface features

and is not the result of the domain structure. The next peak occurs at around 40 nm and corresponds to the domain periodicity. Error bars were estimated by determining the domain periodicity for several areas of the film and averaging the results. Lastly a small broad peak is seen at a domain periodicity of 8 nm which could represent the width of the *a* domains. However, this peak is not clear and for many films it is often not see so a quantitative analysis is difficult.

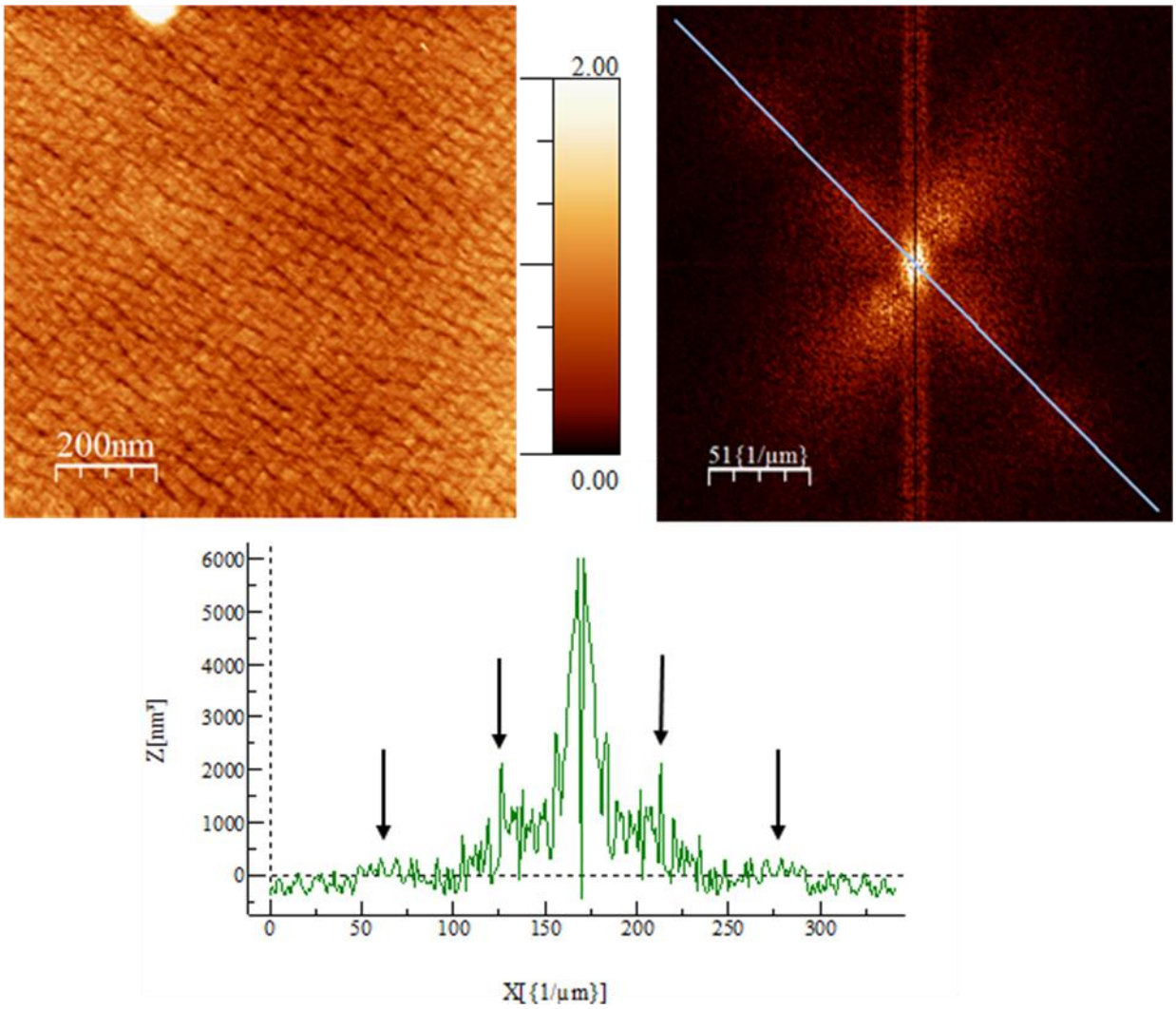

Figure 23. (a) AFM image of $PbTiO_3$ surface, (b) Fast Fourier Transform of image a,(the x axis of the profile corresponds to the total length of the line in the FFT image, so X= ~170 /nm corresponds 0/nm) (c) profile across diagonal of FFT

The resulting domain periodicities for films of different thicknesses is shown in Figure 24. Also plotted in this figure are two trend lines. The solid line corresponds to a square root dependence while the dotted line represents a linear fit. The films seem to fit better with a linear dependence rather than the predicted square root dependence.

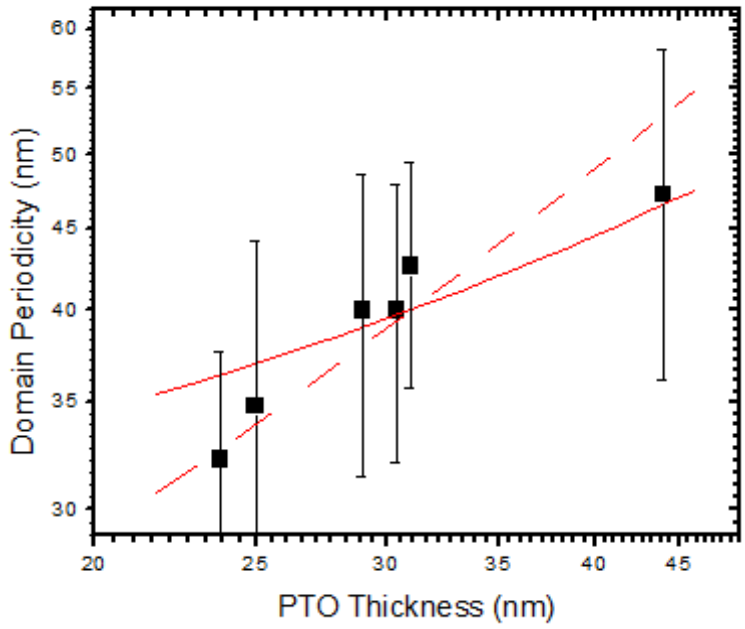

Figure 24. Domain Periodicity vs $PbTiO_3$ thickness, solid line represents square root dependence and dashed line represents linear dependence

A linear dependence between the film thickness and domain periodicity is not predicted using the approach taken by Roytburd. However, a linear dependence is predicted over a limited thickness regime by Pertsev and Zembilgotov. Pertsev and Zembilgotov modeled the strain in the system using a distribution of fictitious dislocations and disinclinations. A schematic of the fictitious dislocations and disinclinations used is shown in Figure 25. Since the strain within each elastic domain is uniform the fictitious dislocation and disinclinations needed to replicate the strain field in the film are localized to the domain boundaries and the interface. In this case, misfit strain is recreated by fictitious dislocations present at the film/substrate interface. The density of the dislocations at the interface changes

depending of the domain. The domain boundaries could be modeled in a similar manner using fictitious dislocations. However, the strain field of such dislocations is the same as the field produced by a pair of straight wedge disinclinations located at the intersection between the domain boundary and the interface [28]. As a result, the strain field produced by the domain boundaries is reproduced by a series of alternating disinclinations with equal but opposite strength.

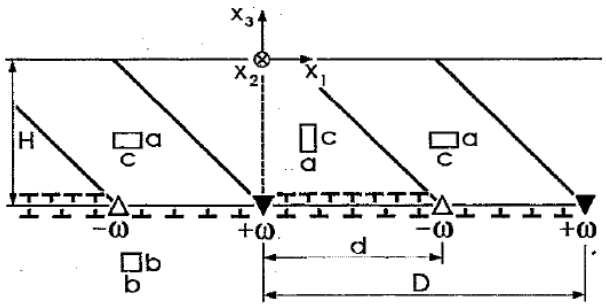

Figure 25. Schematic of 90° domain structure with fictitious dislocations and disinclinations used to model the strain field [16].

The internal energy of the film is calculated from the elastic stresses produced by the array of fictitious dislocations and disinclinations The resulting energy expression is a function of two variables that define the domain structure. These two variables are the ratio of the domain period to the film thickness (D/H), and the volume fraction of *c* domains ($\varphi=d/D$). Equilibrium values for both these variables are calculated by $\partial W/\partial D=0$ and $\partial W/\partial \varphi=0$

The equilibrium domain periodicities for films with different coherency strain are shown in Figure 26 [16]. This theory predicts a non-monotonic dependence between domain periodicity and the film thickness. A local minimum is observed at a normalized thickness of ~4-7 followed by a local maximum at ~20-30. After these two there is a linear relation between the domain periodicity and the film thickness when the normalized film thickness is

greater than 70. For large thicknesses (not shown in this Figure) the square root behavior will return.

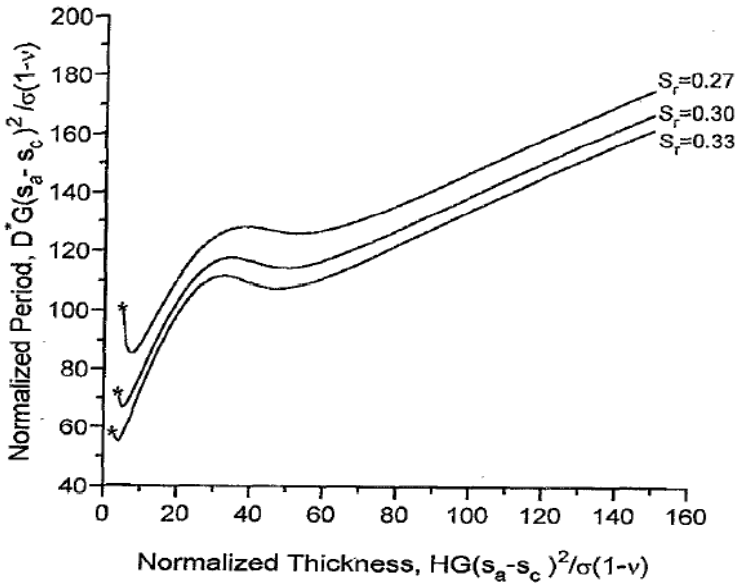

Figure 26. Normalized Period vs. Normalized Thickness for Pertsev and Zembilgotov model [16]

The data obtained in this paper along with results from Ard Vlooswijk [29] are plotted together in Figure 27 with the theoretical predictions from Pertsev and Zembilgotov [16]. The most striking feature is that the theory predicts domain periodicities which are approximately twice as large as the experimental results. Even when the theoretical predictions are reduced to match the experimental results there is still disagreement between the two. For very thin films an increase in the domain periodicity is observed for thin films close to the cross over to 180° domain which is in agreement with theory. However, the local maximum is not observed. Instead it appears the linear region extends all the way down to a periodicity of ~24 nm.

There are several factors which Pertsev and Zembilgotov do not account for which could be causing the discrepancies with the experimental result. First, the energy calculated does not include the energy due to the depolarizing field. The depolarizing field will have a

larger influence for thinner films and could be the reason why the local maximum is not observed. Also, Pertsev and Zembilgotov model assumes the film and substrate to be homogeneous and isotropic. The $DyScO_3$ substrate is psuedocubic so it is not completely isotropic and could be a factor in the observed differences.

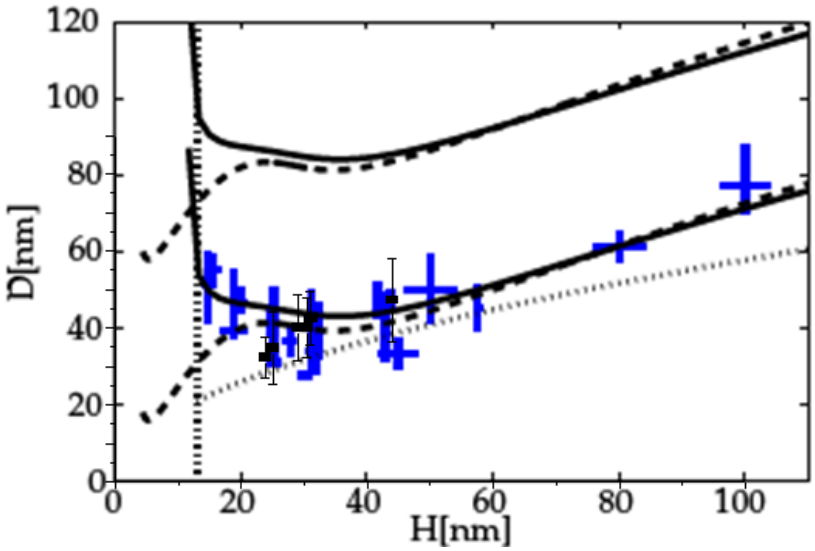

Figure 27. Domain Periodicity (D) vs. Film thickness (H). Vertical dotted line represents cross over from 180° to 90° domains, crosses represent data from Ard Vlooswijk, boxes represent data from this paper. The dotted line represents the theoretical square root dependence from Roytburd with domain wall energy of 100mJ/m2. The upper solid line and upper dashed line represents the theoretical dependence from Pertsev and Zembilgotov, solid corresponds to a fit at room temperature and 27mJ/m2 domain wall energy, dashed line corresponds to fit a 440°C and 17mJ/m2. The lower solid and dashed lines represents the same fits with arbitrary substations of 41nm and 37nm respectively to fit the experimental data. [29]

5. Conclusions

As seen in the results section, all of the $PbTiO_3$ films from 24nm to 44nm had 90° domains structures. The presence of 90° domain structures is confirmed by RSMs and the AFM images of the film surface. The periodicity of the 90° domains is investigated using a FFT of the AFM surface topography. The results show that a linear dependence is a better fit than the theoretical square root dependence. The results are then compared to the theoretical predictions of Pertsev and Zembilgotov. Qualitatively there is good agreement between theory and experiment. Both show a linear dependence for thicker films and an increase in

the domain periodicity close the cross over to 180° domains. However, a local maximum is not observed. Quantitatively the theoretical predictions are approximately twice as large as the experimental data. Deviation from the theoretical predicted behavior is attributed to the influence of the depolarizing field which is the driving force for 180° domains. For sufficiently thin films the influence of the depolarizing field cannot be ignored and the theoretical models only take into account elastic considerations. Further investigation is needed for films with thicknesses close to the crossover between 180° and 90° domains to fully explain the complicated interaction of both elastic and electrostatic effects on the domain periodicity.

Acknowledgments

There are several people I would like to thank for their help in making this thesis possible. First and foremost I want to thank my supervisor Beatriz Noheda. The guidance, support, and constructive criticism I received has not only been invaluable for completing my master's thesis but will also be helpful in the years to come. I want to thank Ard Vlooswijk for teaching me many of the techniques I used for this project including PLD, XRD, and the substrate treatment. In addition Ard was extremely helpful while I was still learning about this topic and was always available and willing to answer any question I had. Thank you to Christophe Daumont for patiently being there and helping whenever I encountered an error message during my PLD depositions. Thanks to Anthony Ferri for teaching me how to perform the AFM and PFM measurements. Thank you to my office matre Gijsbert Rispens for answering any question I had. Thank you to Henk Bruinenberg for repairing the PLD system after I broke it. Finally, I would also like to thank my family and friends, especially Vilija Naruskevic, for their continued support over the duration of this project.

Appendix A $SrRuO_3$ AFM Images

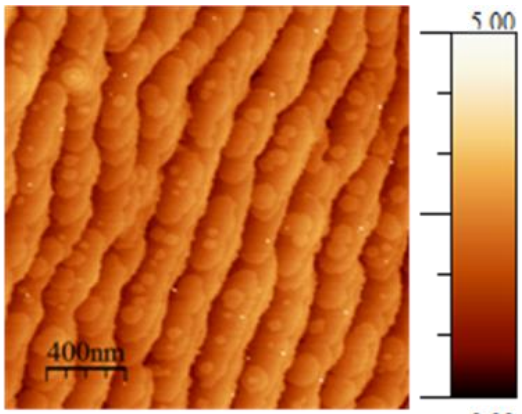

1st Attempt

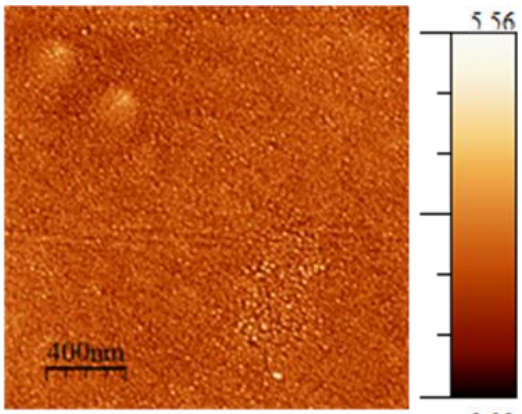

2nd Attempt

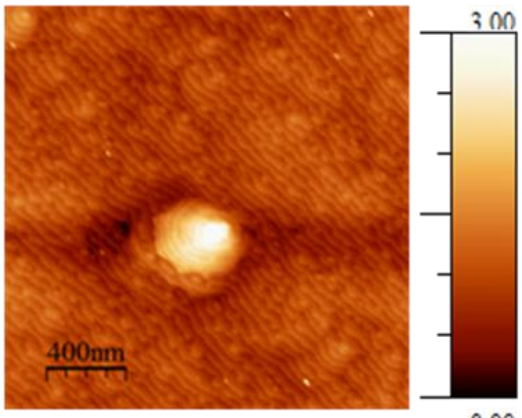

3rd Attempt

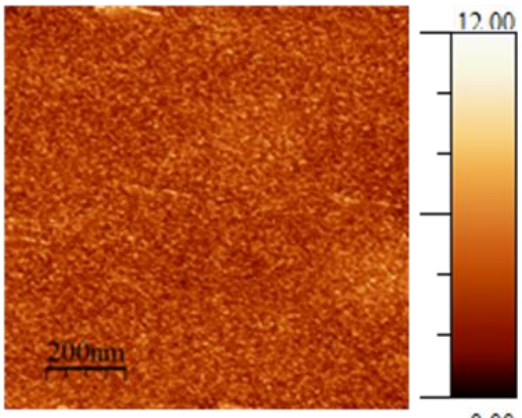

4th Attempt

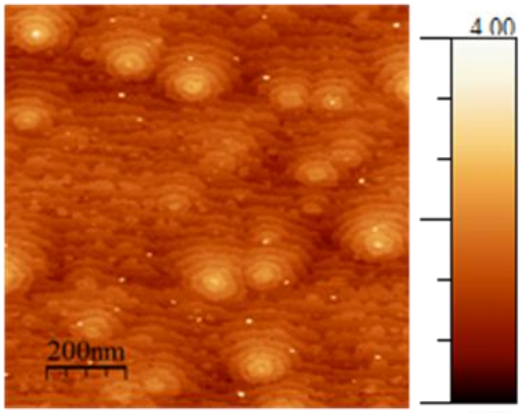

5th Attempt

All scale bars in nm

Appendix B 2θ-ω scans

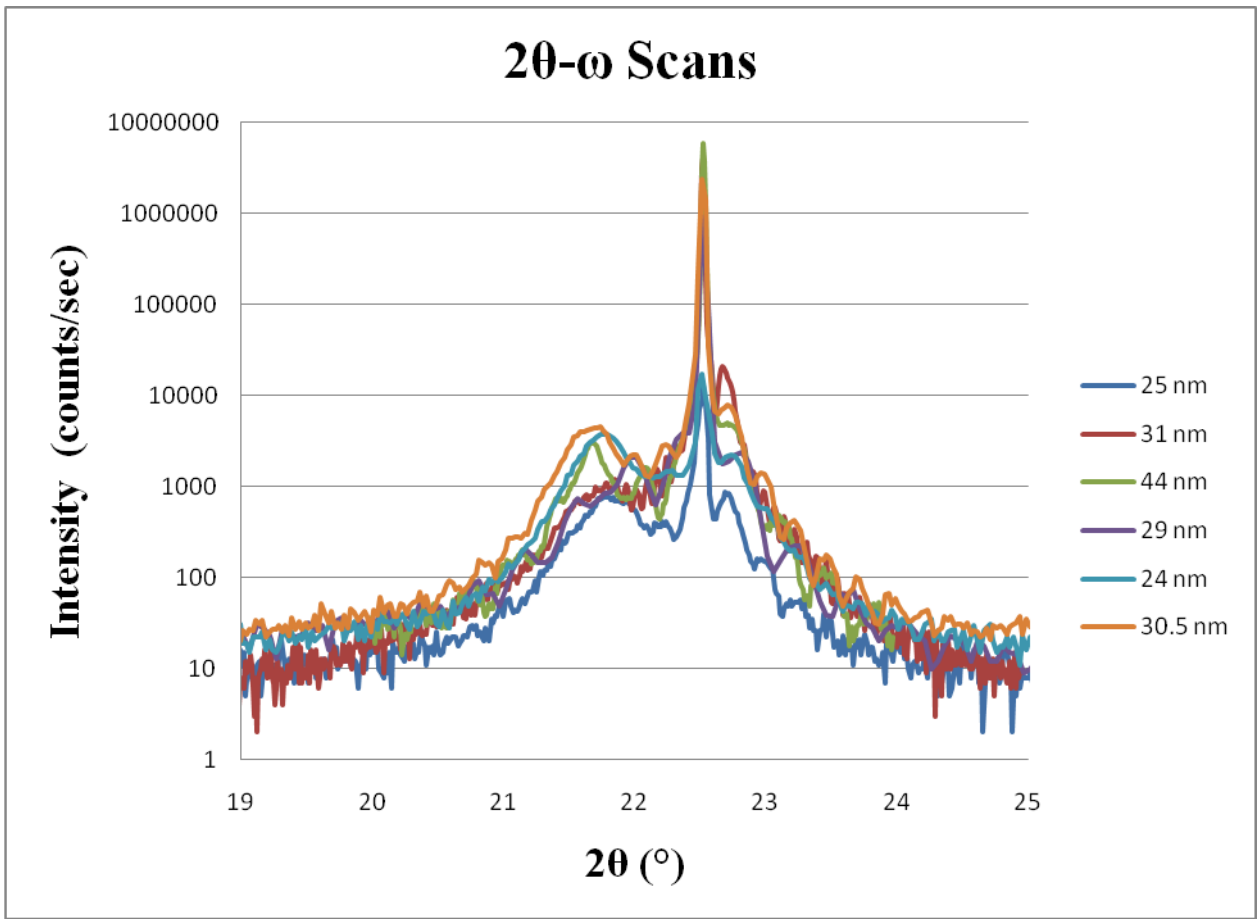

Appendix C $PbTiO_3$ AFM Images

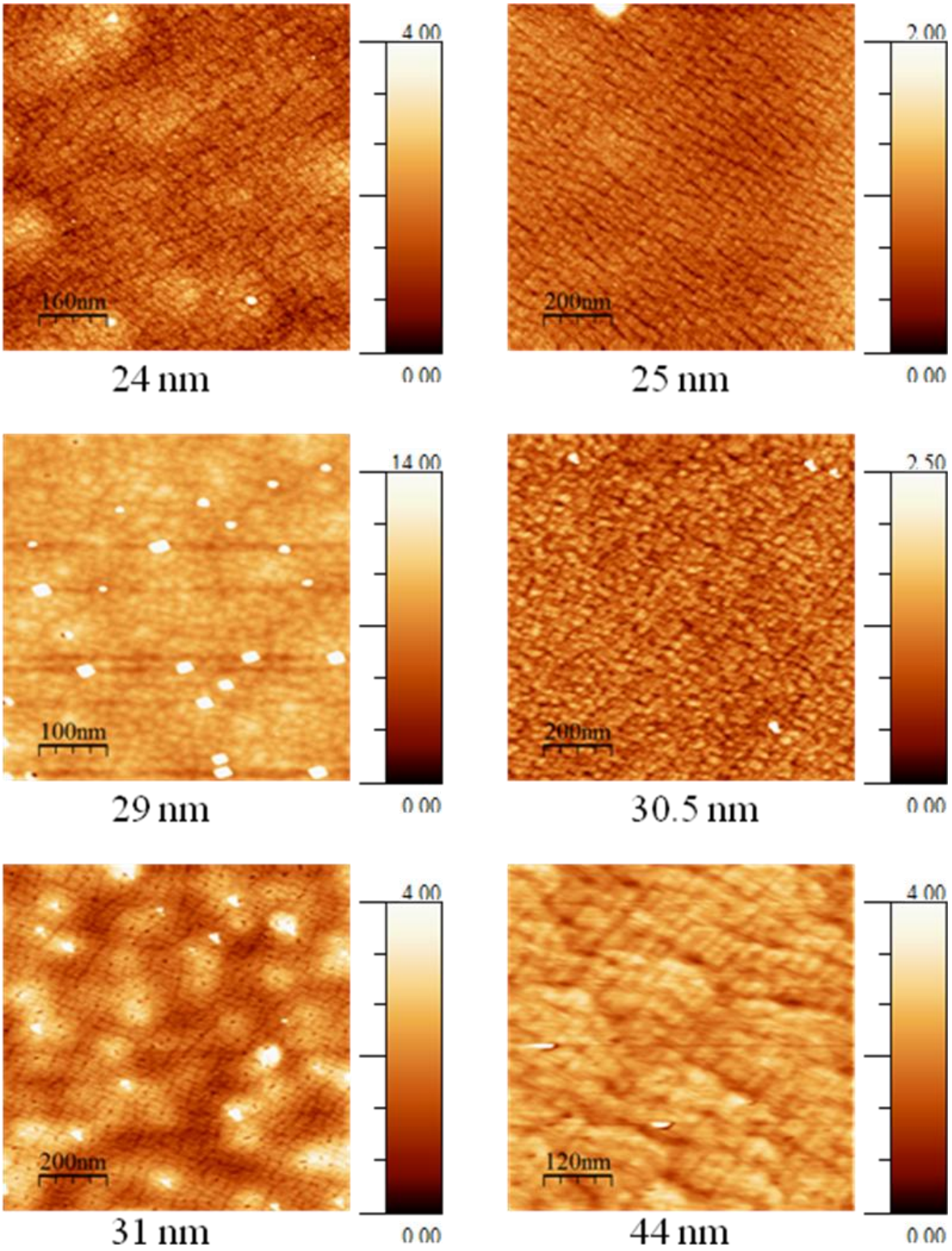

All scale bars in nm

Appendix D $PbTiO_3$ Out of Plane PFM Images

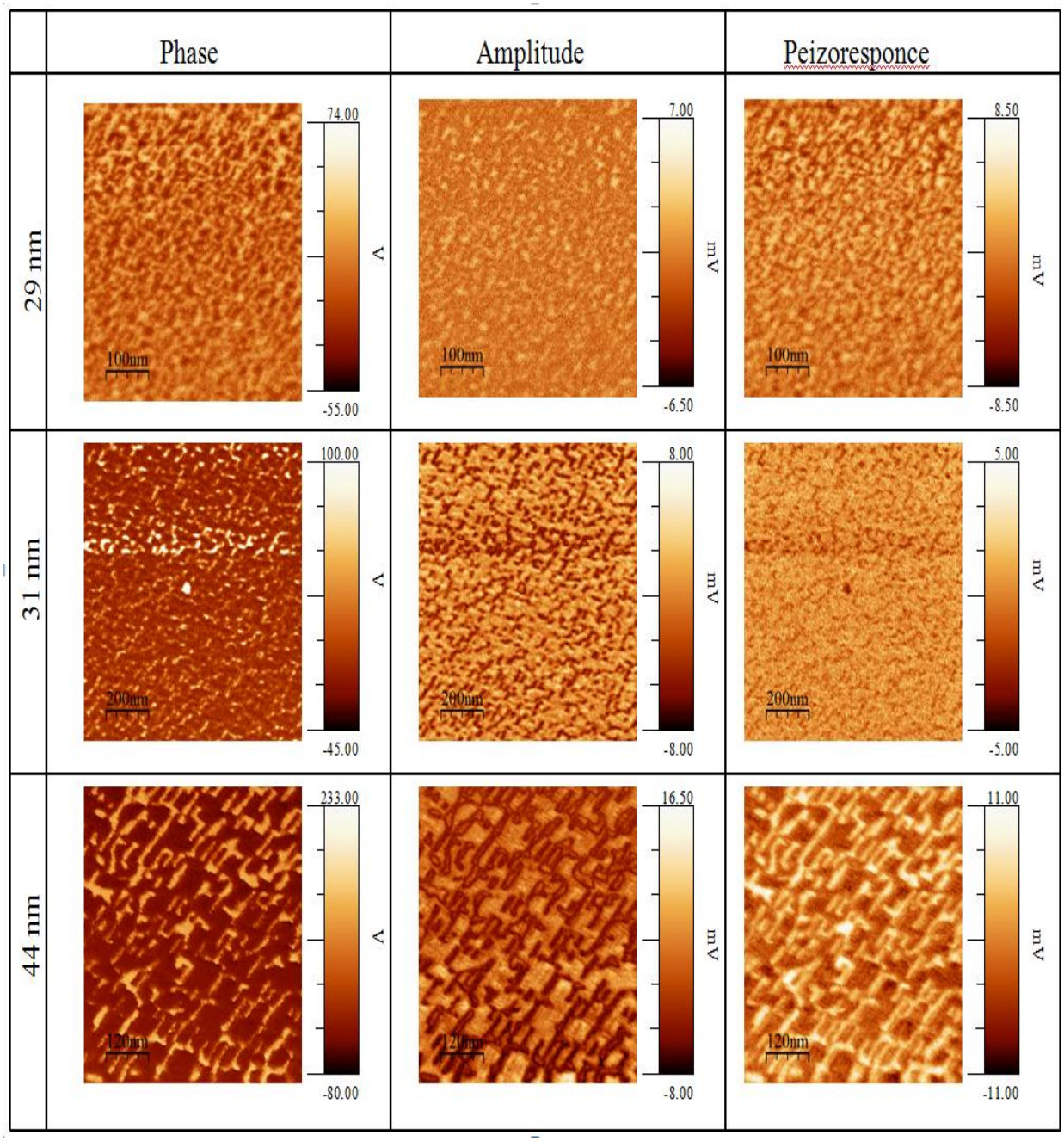

References

[1] J.F. Scott, Science. 315, 954 (2007.)

[2] K. Lee, S. Baik, Annu. Rev. Mater. Res. 36, 81 (2006).

[3] N. Setter et al. J. Appl. Phys. 100, 051606 (2006).

[4] K. S. Lee, J. H. Choi, J. Y. Lee, and S. Baik, J. Appl. Phys. 90, 4095 (2001).

[5] D.D. Fong, C. Thompson, Annu. Rev. Mater. Res. 36, 431 (2006).

[6] R. E. Cohen, Nature 358, 136–138 (1992).

[7] W. Pompe, X. Gong, Z. Suo, and J. S. Speck, J. Appl. Phys. 74, 6012 (1993).

[8] J.S. Speck, W. Pompe , J. Appl. Phys. 76, 466 (1994).

[9] J.W. Mathewes, A.E. Blakeslee, J. Cryst. Growth, 27,118,(1974).

[10] R. People, J.C. Bean, Appl. Phys. Lett. 47, 322, (1985).

[11] A. H. G. Vlooswijk, B. Noheda, G. Catalan, A. Janssens, B. Barcones, G. Rijnders, D. H. A. Blank, S. Venkatesan, B. Kooi, and J. T. M. de Hosson, Appl. Phys. Lett. 91, 112901 (2007).

[12] A. Schilling et. al., Phys. Rev. B., 74, 024115 (2006)

[13] C. Kittel, Phys. Rev., 70, 965, (1946)

[14] T. Mitsui, J. Furuichi, Phys. Rev., 90, 193, (1953)

[15] A. Roytburd, Phys. Stat. Sol. A, 37, 329, (1976)

[16] N.A. Pertsev, A.G. Zembilgotov, J. Appl. Phys., 78, 6170, (1995)

[17] N. A. Pertsev, A. G. Zembilgotov, A. K. Tagantsev, Phys. Rev. Lett., 80, 1988, (1998)

[18] David P. Norton. "Pulsed Laser Deposition of Complex Materials; Towards Practical Applications." Pulsed laser deposition of thin films: Applications-led growth of functional. Robert Eason. Wiley-Interscience. 2006.

[19] A. Inam et. al., Appl. Phys. Lett., 53, 908, (1988)

[20] G. Rijnders, D. H.A. Blank. "Growth Kinetics During Pulsed Laser Deposition." Pulsed laser deposition of thin films: Applications-led growth of functional. Robert Eason. Wiley-Interscience. 2006.

[21] G. Rijnders, A.J.H.M. and Blank, "Real-time growth monitoring by high-pressure RHEED during Pulsed Laser Deposition." Thin Films and Hetereostructures for Oxide Electronics.Satischandra B. Ogale Springer Science + Business Media, Inc. 2005.

[22] G. Rijnders, D. H.A. Blank. "In situ Diagnostics by High-Pressure RHEED During PLD." Pulsed laser deposition of thin films: Applications-led growth of functional. Robert Eason. Wiley-Interscience. 2006.

[23] C. Daumont. *Multiferroic Perovskites Under Epitaxial Strain: The Case of $TbMnO_3$ thin films.* PhD thesis. Rijksuniversiteit Groningen. The Netherlands (2009)

[24] M. Birkholz, P.. Fewster, C. Genzel, Thin Film Analysis by X-Ray Scattering. Wiley-VCH, 2006.

[25] A. L. Kholkin , S. V. Kalinin, A. Roelofs, A. Gruverman "Review of Ferroelectric Domain Imaging by Piezoresponse Force Microscopy." Scanning Probe Microscopy:

Electrical and Electromechanical Phenomena at the Nanoscale. S. V. Kalinin, A. Gruverman. Springer, 2006.

[26] A. Gruverman, S.V. Kalinin, J. of Mater. Sci., 41, 107, (2006).

[27] A.F. Devonshire, Adv Phys., 3, 85, (1954).

[28] R. de Wit, J. Natl. Bur. Stand. A, 77, 607, 1973

[29] A. Vlooswijk, *Structure and Domain Formation in Ferroelectric Thin Films.* PhD thesis. Rijksuniversiteit Groningen. The Netherlands (2009)